Available online at www.sciencedirect.com

jmr&t Journal of Materials Research and Technology

journal homepage: www.elsevier.com/locate/jmrt

Original Article

Effects of CrMnFeCoNi additions on microstructure, mechanical properties and wear resistance of Ti(C,N)-based cermets

Shandong Yang [a,b], *Ji Xiong* [a,b,*], *Zhixing Guo* [a], *Biao Wu* [a], *Tian'en Yang* [a], *Qianbing You* [a], *Junbo Liu* [a,c], *Chengjun Deng* [a], *Ding Fang* [d], *Shaoxuan Gou* [d], *Ze Yu* [d], *Sitao Chen* [d]

[a] *School of Mechanical Engineering, Sichuan University, Chengdu, 610065, PR China*
[b] *Yibin Industrial Technology Research Institute of Sichuan University, Yibin, 644000, PR China*
[c] *School of Mechanical & Aerospace Engineering, Nanyang Technological University, 50 Nanyang Avenue, 639798, Singapore*
[d] *Chengdu Aircraft Industrial (Group) Co., Ltd, Chengdu, 610017, PR China*

ARTICLE INFO

Article history:
Received 14 December 2021
Accepted 3 February 2022
Available online 10 February 2022

Keywords:
Ti(C,N)-based cermets
CrMnFeCoNi/Ni binders
Microstructure
Wear resistance
Cutting properties

ABSTRACT

Ti(C,N)-xCrMnFeCoNi-(15wt.%-x)Ni cermets (x = 0wt.%, 5wt.%, 10wt.%, 15wt.%) were fabricated by low-pressure sintering. Because of the sluggish diffusion effect of high-entropy alloy (HEA), the grain growth of cermets containing HEA binder is inhibited. The FCC binder phases of cermets with CrMnFeCoNi/Ni binders generate a uniform dispersion, motivating to form many complete and moderate rim phases and wet the ceramic particles. Furthermore, the hardness of cermets roughly increases, while the strength and fracture toughness maintain the change tendency of rising the peak and then falling with CrMnFeCoNi additions. Ti(C,N)-5wt.% CrMnFeCoNi-10wt.% Ni cermets obtains a prominent mechanical property combination with hardness of 1646 ± 13.5 HV_{30}, strength of 2181 ± 167.2 MPa and fracture toughness of 9.1 ± 0.11 MPa $m^{1/2}$. Besides, the cermets containing CrMnFeCoNi/Ni binders obtain reduced friction coefficients and low wear rates at 750 °C compared with Ti(C,N)–Ni cermets and Ti(C,N)-HEA cermets. The superior high-temperature wear resistance is ascribed to the thermal softening resistance of CrMnFeCoNi, strengthening and toughening effect of CrMnFeCoNi/Ni on matrix and the transition of wear mechanism from abrasive wear and the removal of tribochemical layers to the removal of tribochemical layers. The cutting lifetime of cermets containing CrMnFeCoNi/Ni binders is increased by 40%–70% in comparison with Ti(C,N)–Ni cermets during machining 17-4 PH stainless steel. Concisely, Ti(C,N)-based cermets with outstanding mechanical, wear resistance and cutting properties can be obtained by partially replacing Ni with 5–10 wt.% CrMnFeCoNi.

© 2022 The Author(s). Published by Elsevier B.V. This is an open access article under the CC BY-NC-ND license (http://creativecommons.org/licenses/by-nc-nd/4.0/).

* Corresponding author.
E-mail address: 13668149296@163.com (J. Xiong).

https://doi.org/10.1016/j.jmrt.2022.02.021

2238-7854/© 2022 The Author(s). Published by Elsevier B.V. This is an open access article under the CC BY-NC-ND license (http://creativecommons.org/licenses/by-nc-nd/4.0/).

1. Introduction

Ti(C,N)-based cermets are a kind of composite material with ceramic hard phase and metal binder phase, possessing both plastic toughness of metal and wear resistance of ceramics. As effective substitutes for cemented carbides, Ti(C,N)-based cermets have been popularly applied to the cutting and grinding tools on account of the high hot hardness, good wear resistance, low friction coefficient and superior chemical stability [1–4]. In the service process, cermet cutting tools are up against the complex working conditions, such as tribological behavior, high temperature, stress and so on. Especially, the service temperatures usually exceed 600 °C for dry high-speed cutting application, which results in severe wear of cutting tools accompanied by the oxidation [5]. Under these relatively harsh conditions, high temperature performance of cermets becomes the dominant factor to determine the cutting performance and durability of tools.

Although the minor metal binder is added to cermets, it plays a crucial part in the microstructure and properties of cermets, which can make a contribution to the fracture toughness. However, considering that Ti(C,N)-based cermets are usually exposed to high-temperature and tribological environments during operation, the traditional binder metals (including Ni, Co and Fe etc.) display poor softening resistance and inadequate oxidation resistance [6,7]. When the softening binder phase in cermets is firstly wiped away during service process, the resistance to plastic deformation decreases sharply, which can reduce the service life of cutting tools and damage the surface quality of cutting workpieces. Therefore, it is an essential approach to expand the application of cermets by developing a novel metal binder with the better high-temperature performance [8–10]. In recent years, high entropy alloys (HEAs), proposed firstly by Yeh et al. [11], have been postulated to enhance cemented carbides and cermets as binders [12–17].

High entropy alloys (HEAs), which contain at least five principal components in equal or near-equal proportions (5-35atom%), are mainly simple solid solution (SS) phases with body-centered-cubic (BCC) or face-centered-cubic (FCC) structure [11,18]. As a newly burgeoning family of alloys, due to their vast exploration space and excellent high-temperature wear resistance and high-temperature oxidation resistance derived from the four core effects compared with conventional alloys, some HEA systems have been presumed as metal binders of cermets. Zhu et al. [19] synthesized novel Ti(C,N)–AlCoCrFeNi cermets, which have superior high-temperature oxidation resistance compared with cermets with Ni/Co binders. A.G.de la Obra et al. [20] investigated that microstructurally simple (Ti,Ta,Nb) (C,N)–CoCrFeNiMn and (Ti,Ta,Nb) (C,N)–CoCrFeNiV cermets obtain lower than expected hardness and fracture toughness due to the poor densification. Subsequently, the authors researched that the proportions of Cr, Cu, Mn, V decrease slightly compared with the original proportions in four novel Ti(C,N)-based cermets containing CoCrCuFeNi, CoCrFeNiV, CoCrFeMnNi and CoFeMnNiV binders because of the element segregation and sublimation of HEAs during high temperature sintering [21]. Fang et al. [22] reported that Ti(C,N)–$Al_{0.3}$CoCrFeNi cermets gain the higher hardness and fracture toughness, at the same time, improve the oxidation resistance and wear resistance at high temperature compared with Ti(C,N)–Ni/Co cermets. Nevertheless, the cermets/cermeted carbides containing pure HEA binder generally appear high residual porosity and possess fractionally enhanced comprehensive mechanical properties. The issue is deemed to be due to the HEA binder's poor wetting capacity towards the hard phase and element loss of HEAs during high temperature sintering [13,20,21,23]. Hence, partially adding HEA as binders is a potential method to strengthen and toughen cermets under the condition of maintaining good wettability.

In this paper, it is proposed that Ni is partially replaced by adding gas atomized CrMnFeCoNi HEA powders as binders to reinforce Ti(C,N)-based cermets. Ti(C,N)-xCrMnFeCoNi-(15wt.%-x)Ni cermets (x = 0wt.%, 5wt.%, 10wt.%, 15wt.%) were fabricated and the co-effects of CrMnFeCoNi/Ni binders on the microstructure, mechanical properties, high-temperature friction and wear performances and cutting properties of cermets were investigated.

2. Experimental procedure

2.1. Sample preparation

The CrMnFeCoNi HEA powders were prepared by the gas atomization method through using Cr (purity>99.8%), Mn (purity>99.9%), Fe (purity>99.8%), Co (purity>99.9%) and Ni (purity>99.8%) metals as raw materials from Jiangsu Vilory Advanced Materials Technology Co., Ltd of China. The bulks of Cr, Mn, Fe, Co and Ni were melted in a high-frequency induction furnace. Then, the atomized CrMnFeCoNi liquid mixture was split into the spherical droplets under an argon pressure of 4 MPa. After cooling, the solidified HEA powders were collected by the airtight volume collector. The chemical compositions (at.%) of gas atomized CrMnFeCoNi powders are shown in Table 1.

Ti(C,N)-based cermets were synthesized through a standard powder metallurgy method. The basic compositions (wt.%) of series of cermets are listed in Table 2. Binder powders were blended with Ti($C_{0.7}$,$N_{0.3}$) (1.20 μm), WC (1.00 μm), Mo_2C (1.75 μm), TaC (1.25 μm) in the grinding tank with cemented carbides balls (powder-to-ball ratio of 1: 10) and industrial gasoline as grinding medium, and then rotated for 72 h at 56 rpm on a roller ball mill. Then, the mixture slurry was dried in a vacuum evaporator at 100 °C and sieved by a 60-mesh filter. Subsequently, under the 250 MPa uniaxial pressure, the mixed powders were pressed into the required green bodies. The size of the rectangular green bodies was about 5.25 mm × 6.5 mm × 20.00 mm. Finally, the green samples were sintered through vacuum sintering (vacuum degree

Table 1 – Compositions (at.%) of gas atomized CrMnFeCoNi powders.

Elements	Cr	Mn	Fe	Co	Ni
Nominal	20	20	20	20	20
Actual	19.73	19.63	19.85	20.94	19.85

Table 2 – Compositions (wt.%) of series of cermets.

Cermets	$Ti(C_{0.7},N_{0.3})$	WC	TaC	Mo_2C	Ni	CrMnFeCoNi
CH0	Balance	19	2	4	15	0
CH1	Balance	19	2	4	10	5
CH2	Balance	19	2	4	5	10
CH3	Balance	19	2	4	0	15

5–40 Pa) at 1310 °C for 0.5 h, and then through low-pressure sintering with the argon atmosphere of 5 MPa at 1440 °C for 1 h. The sintered samples were first ground with 3000 # diamond grinding disc and then polished with 2.5 μm diamond paste for subsequent experiments.

2.2. Sliding wear tests

The sliding friction and wear tests were conducted on a high-temperature tribometer (Model HT-1000, Lanzhou, China). In order to fully evaluate the wear resistance potential of cermets, the Si_3N_4 balls (diameter 6 mm; hardness ~ 1700 HV) are selected as the counterbody. The cutting temperature field of inserts is simulated by the Third Wave AdvantEdge. As presented in Fig. 7, accordingly, the test temperature during sliding is 750 °C. Test parameters were chosen with the applied load of 10 N, the rotating speed of 1000 rpm, the sliding time of 30 min. The wear volume (V) of specimens were detected via the Optical Profiler (Model Contour GT-K1, USA). Next the wear rate (W) is obtained by the following expression:

$$W = V/(F_N \cdot \nu_S \cdot t) \quad (1)$$

where V represents the wear volume, F_N represents the applied load, υ_S represents the sliding speed and t represents the sliding time.

2.3. Cutting tests

The dry cutting tests of the cermet inserts were carried out on the CNC lathe (Model CK6140, China) on 17-4 PH stainless steel bar (the initial diameter 80 mm). The cutting parameters were chosen with the cutting depth of 0.5 mm, cutting speed of 120 m/min and feed rate of 0.06 mm/rev, respectively. The VMS-3020F imager was implemented to measure the flank wear values of inserts.

2.4. Characterization

The phase structures of binder powders and sintered cermets were detected by X-ray diffraction (XRD, Philips PW-1700) with copper Kα radioactive source. The microstructure and wear morphology of cermets and inserts were observed through the scanning electron microscopy (Model Hitachi S-4800) carried with the energy dispersive spectrometer (EDS) and the grain size and orientation were detected by electron backscatter diffraction (EBSD). The density of as-sintered cermets was measured by a high-precision balance with water media at 20 °C based on Archimedes principle. The strength (TRS) of samples (size 5.25 × 6.5 × 20.00 mm) was acquired via the testing instrument (Model WE-100B, China) with a loading rate of 0.5 mm/min and a span of 16 mm. The hardness (HV_{30}) and

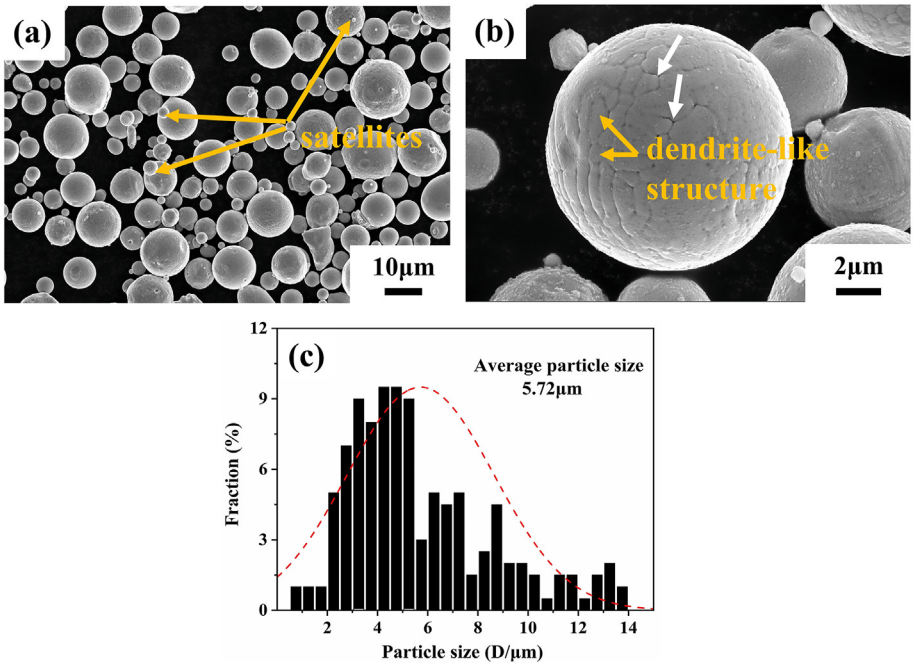

Fig. 1 – SEM micrographs and particle size distributions of the gas-atomized CoCrFeMnNi powders.

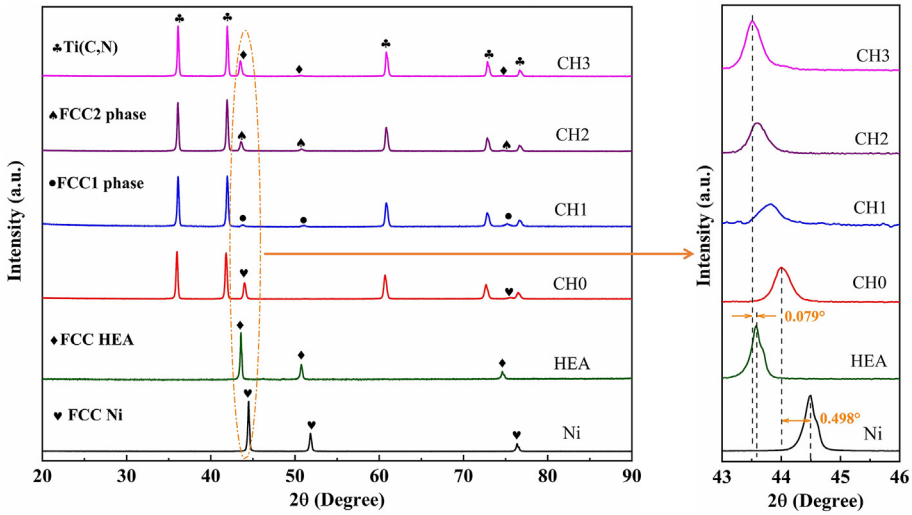

Fig. 2 – XRD patterns of the initial binder powders and cermets CH0, CH1, CH2 and CH3 after low-pressure sintering.

fracture toughness (K_{IC}) were measured by using a hardness tester under a load of 30 kg for 15 s. Then, the calculated equation of K_{IC} values is as follows [24] :

$$K_{IC} = 0.15\sqrt{\frac{HV_{30}}{\sum_{i=1}^{4} L_i}} \quad (2)$$

where HV_{30} denotes the Vickers hardness and L (mm) denotes the total length of cracks. The values of all mechanical properties and their errors were obtained by calculating the arithmetic mean and standard deviation from five samples (Mean ± S.D.) by using the OriginPro software.

3. Results and discussion

3.1. Phase and microstructure

Fig. 1 demonstrates the SEM of gas atomized CrMnFeCoNi HEA powders as binders. The powders generally show a regular spherical morphology. A satellite structure with large particles adhered by small particles is formed. The statistical result displays that the particle size is mainly distributed in 1–14 μm and the mean particle size is 5.72 μm (Fig. 1c). Under the high magnification SEM, the structure of spherical powders is a

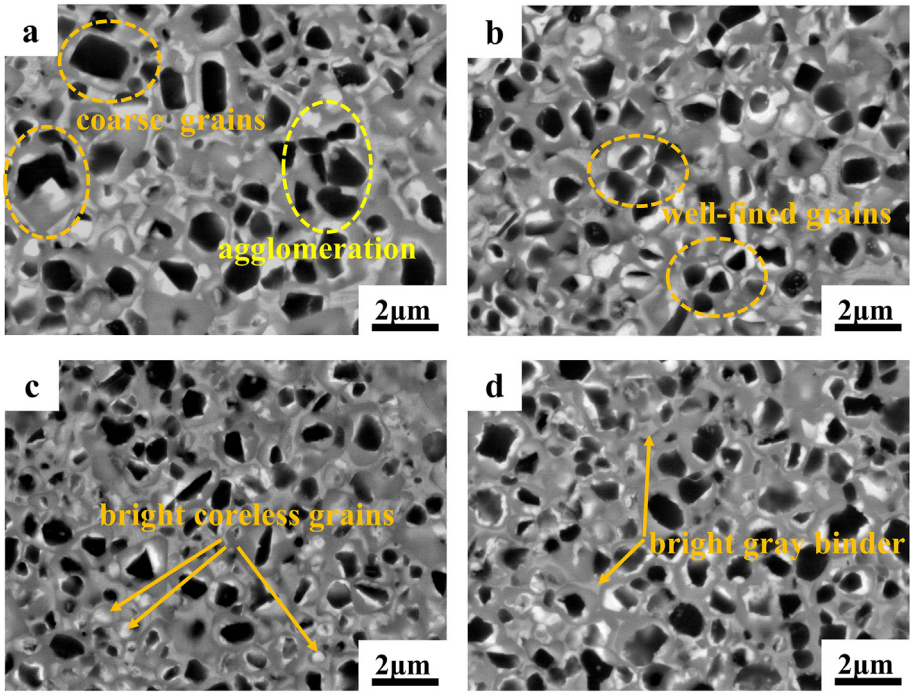

Fig. 3 – Back-scattered SEM images of sintered Ti(C,N)-based cermets with different binders: (a) cermet CH0; (b) cermet CH1; (c)cermet CH2; (d) cermet CH3.

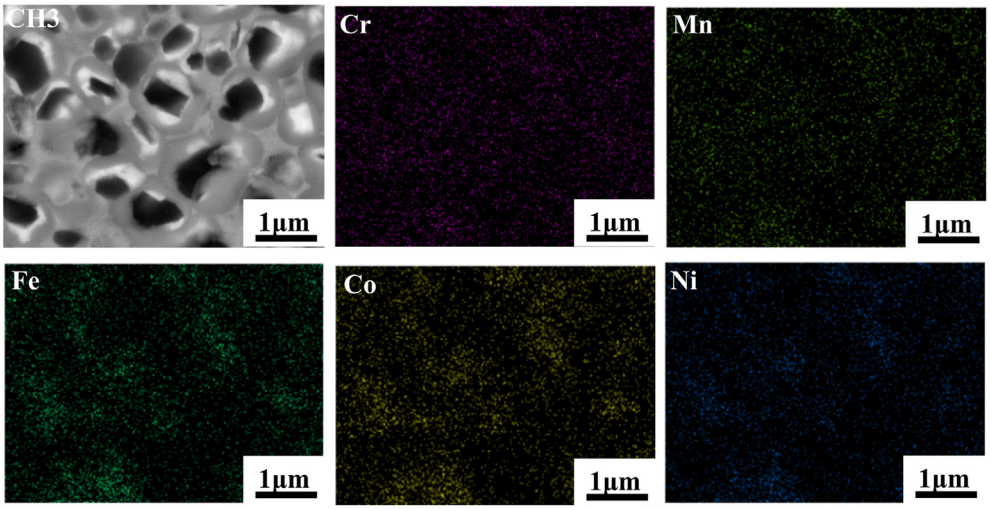

Fig. 4 – The EDS mappings of cermet CH3.

well-fined dendritic structure with the pores formed by the solidification shrinkage of highly viscous melt (Fig. 1b). The satellite structures and pores in dendritic structures are considered to affect the density of parts prepared by adding these HEA powders as raw material [25].

The XRD patterns of Ni, CrMnFeCoNi powders and sintered cermets are shown in Fig. 2. Both Ni and CrMnFeCoNi powders exhibit a simple FCC crystal structure. The four sintered cermets are formed from Ti(C,N) phase and the corresponding FCC binder phase. Apparently, the diffraction peaks of FCC Ni phase of cermet CH0 and FCC HEA phase of cermet CH3 shift to lower diffraction angles in comparison that of Ni and HEA powders. The lattice parameters of Ni phase before and after sintering are 3.524 Å, 3.567 Å, respectively, while HEA phase before and after sintering are 3.592 Å and 3.608 Å, respectively. The lattice constants of binder phases increase after sintering, which is due to the dissolution of Ti, Ta, W and Mo atoms into the binder phase solid solution. And the small increase of HEA phase's lattice parameter in CH3 implies that only a few Ti, Ta, Mo and W atoms dissolve into HEA binder phase on account of the sluggish diffusion of CrMnFeCoNi.

The Bragg angles of FCC binder phases in cermet CH1 and CH2 are between the angles of CH0 and CH3, meanwhile the diffraction peaks widen and the intensity decreases. The solid solution reaction occurs between binder Ni and HEA in addition to hard atoms dissolve in the binder phase during high temperature sintering. For the binder lattice, there are severe local atomic distortions and lattice strains led by the atomic size mismatch and various local atomic environments, affecting a broadening of the diffraction peaks and a reduction in the intensity of the peaks. The binders of cermets CH1 and CH2 obtain relatively high configurational entropy from complex, concentrated components, tending to stabilize the single SS phases. According to the relevant literature [26], the addition of Ni can stabilize FCC phase, and in Cr–Mn–Fe–Co–Ni system, the FCC SS phase can show high temperature stability when the content of Ni is between 10% and 92%. Hence, both bonding phases in cermet CH1 and CH2 show a single FCC SS phase.

Fig. 3 depicts the SEM images of as-sintered cermets. The microstructures of all cermets show the typical core-rim structures surrounded by the bright gray binder phases, which include black core-white inner rim-gray outer rim structures and bright coreless-gray rim structures [27]. The agglomeration of black cores and abnormally coarse grains are found in cermet CH0 (Fig. 3a). Different black cores are even connected together, which forms the incomplete rims. In cermets CH1, CH2 (Fig. 3b, c), many refined black core-white inner rim-gray outer rim grains with intact structure and moderate rim phase thickness are formed. The complete and moderate rim phase is conductive to the good wetting capacity of the binder phase on ceramic grains. However, some incomplete rim phases and rough core-rim structures appear in cermet CH3 (Fig. 3d), which may be attributed to the poor wettability of excess HEA binder on hard phase.

Elements of binder phases in cermets CH0, CH1, CH2 and CH3 detected by EDS are listed in Table 3. The binder solid solutions are poor in hard Ti, Ta, W and Mo atoms, and the less (Ti, Ta, Mo, W) hard phase elements are dissolved in binder phases of cermets adding HEA. The sluggish synergistic diffusion effect of binder phase restrains the dissolution and precipitation process of hard particles [28]. It is worth noting that the binders of cermets adding HEA are deficient in Cr and Mn elements. The EDS mappings of cermet CH3 are depicted in Fig. 4. The distribution of binder elements is slightly different in Fig. 4. The elements Fe, Co and Ni are homogeneously distributed along the binder phases. The Mn mapping differs from the other binder elements and the content is lower than the nominal. This may be because Mn with low melting point evaporates during high temperature sintering [21]. The Cr is slightly segregated into the core-rim structure, which derives from the spinodal decomposition [29].

To further reveal the co-effects of CrMnFeCoNi/Ni binders on cermets, electron back scattered diffraction (EBSD) is employed to detect the morphology and grain orientation of different phases. Fig. 5 displays the SEM/EBSD result of the orientation image map (OIM) at [100] and grain size distribution of as-sintered cermets. From Fig. 5 (a1–d1), the difference

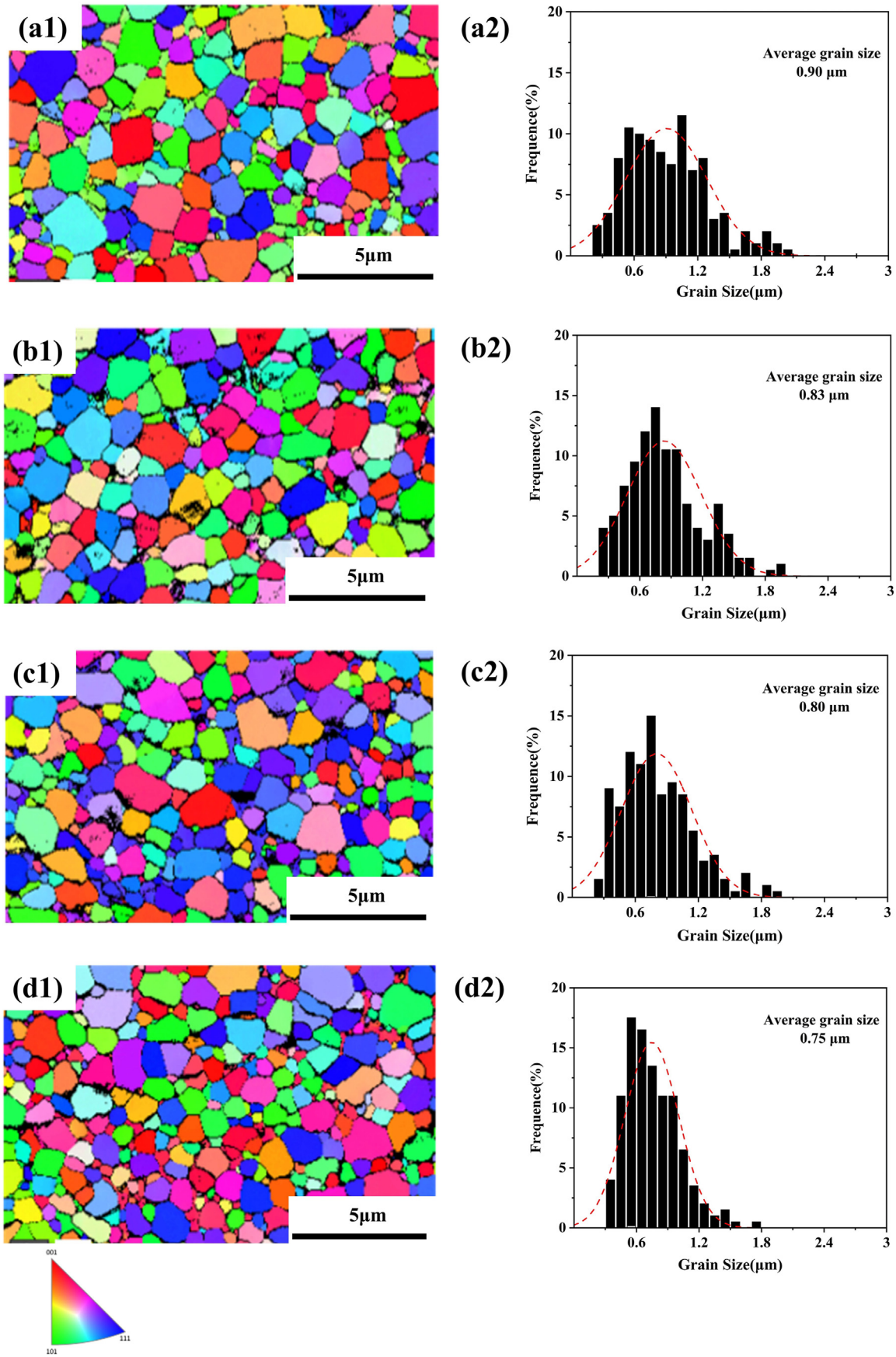

Fig. 5 – SEM/EBSD measurement of the orientation image map (OIM) at [100] for the cermets. (a1-d1) EBSD patterns of corresponding cermets. (a2-d2) Grain size distribution of cermets CH0–CH3.

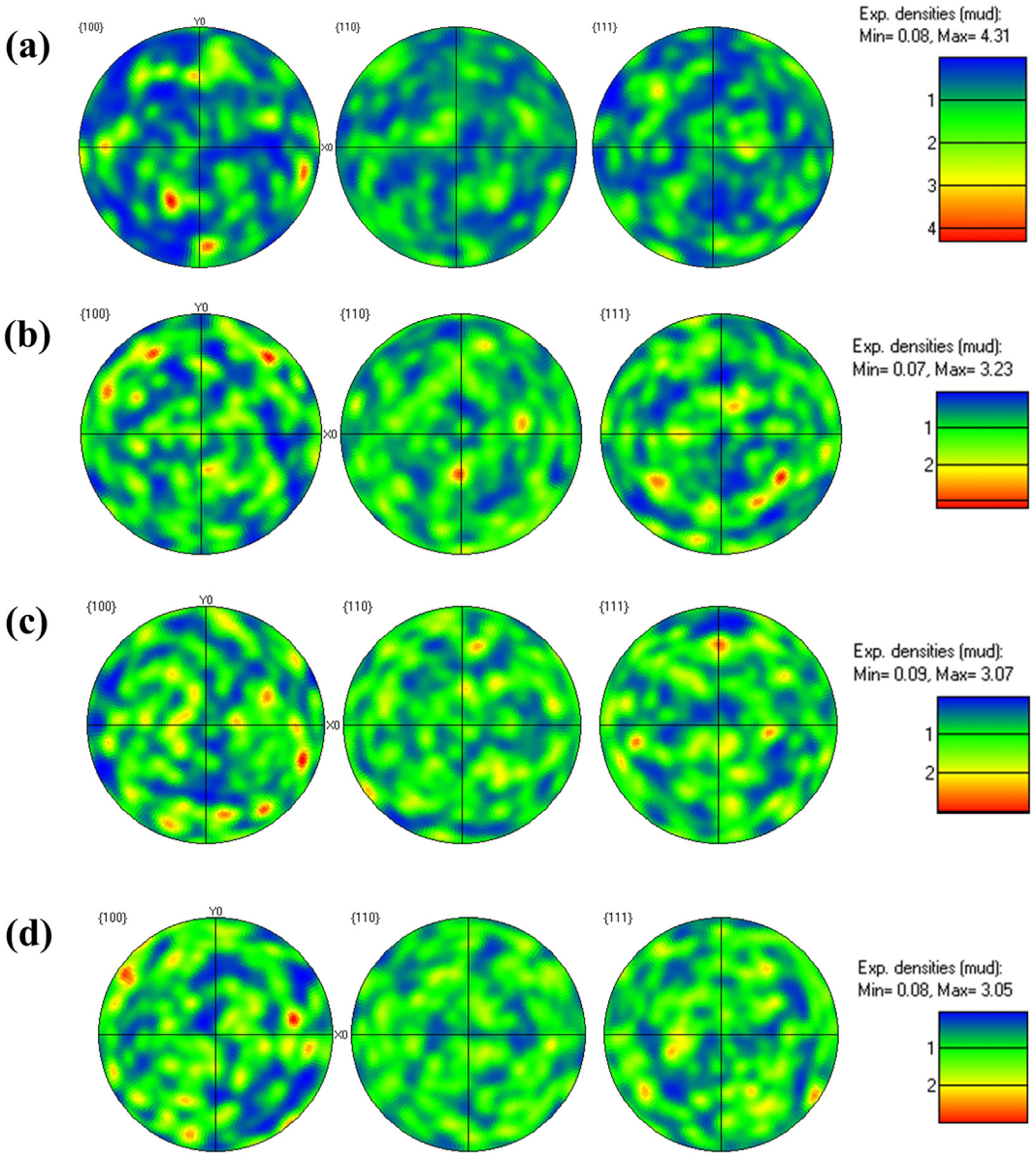

Fig. 6 – The pole figures of hard phases: (a) cermet CH0; (b) cermet CH1; (c) cermet CH2; (d) cermet CH3.

of contrast discloses different crystal orientations, that is, the addition of HEA affects grain orientations of cermets. The statistical diagrams of grain size of corresponding cermets are shown in Fig. 5 (a2–d2). The result illustrates that cermets containing HEA binder have fewer abnormally coarse grains and more uniform grain size distribution. The average grain sizes of cermets CH0, CH1, CH2 and CH3 are 0.90 μm, 0.83 μm, 0.80 μm and 0.75 μm, respectively. With the increment of CrMnFeCoNi content, the mean grain size of cermets decreases, indicating that the binder HEA inhibits the grain growth. The grain growth is usually controlled by the diffusion of dissolved particles through the molten binder phase during the liquid phase sintering [30]. Compared with pure Ni binder, the sluggish diffusion effect of CrMnFeCoNi inhibits the dissolution of hard particles in the liquid phase. Meanwhile, the sluggish diffusion of HEA results in the more difficult collaborative diffusion between different atoms when hard particles are re-precipitated from the binder. In addition, the inherent and severe lattice distortion of CrMnFeCoNi increases the strain energy, which reduces the growth activation energy of hard particles, thus inhibiting the grain growth rate [14]. With an increment of HEA content, the inhibition becomes more significant, and the corresponding mean grain size of cermets becomes smaller. The pole figures (PF) of the hard phases are displayed in Fig. 6. The hard phases of cermets CH0, CH1, CH2 and CH3 exhibit the stronger texture intensity in the (100) PF map, and the maximum texture intensities roughly decrease with the addition of HEA, about 4.31, 3.23, 3.07 and 3.05, respectively.

The distribution of binder phase (green part in Fig) based on EBSD pattern is shown in Fig. 7. It is confirmed that the evolution of FCC binder phase in cermets is mainly distributed

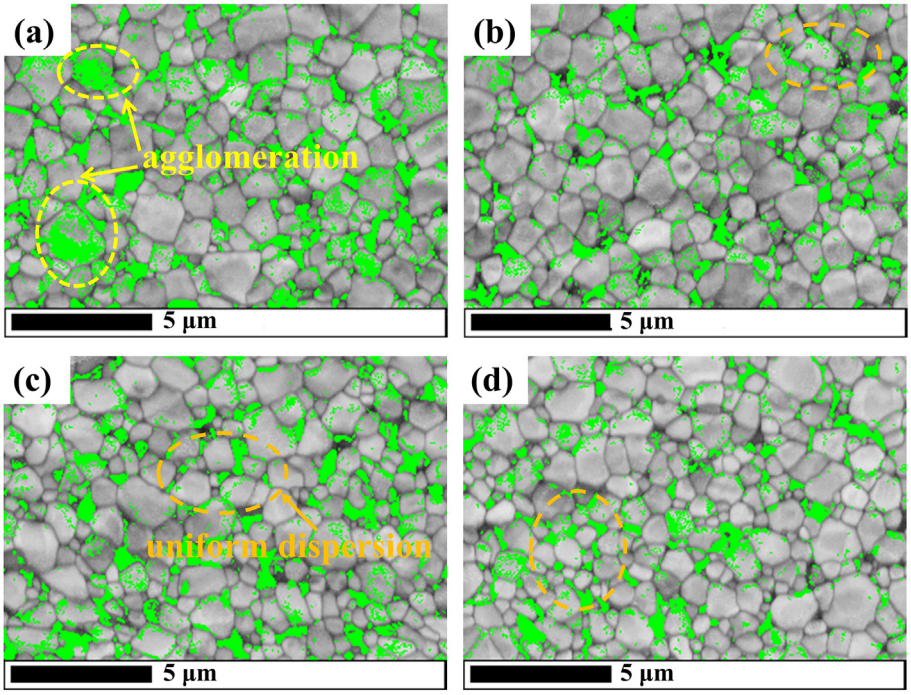

Fig. 7 – Distribution of binder phase in the cermets (The green part is indicated as the FCC binder phase). (a) cermet CH0; (b) cermet CH1; (c) cermet CH2; (d) cermet CH3.

at the grain boundary. A typical structure in which the ceramic phase is embedded in binder phase is formed. Furthermore, the addition of HEA affects the dispersion of binder phase. The agglomeration of binder phase appears in cermet CH0, while the binder phases in cermets CH1 and CH2 are uniformly dispersed compared with cermet CH0. As described in Fig. 7, the mean binder phase thickness (average free path) around hard phase particles in CH0 is larger in comparison with cermets CH1, CH2 and CH3, generally resulting in the reduced hardness [31,32]. Because of the formation of a relatively low-melting eutectic phase in cermets containing CrMnFeCoNi/Ni binders at high temperature and the distortion energy coming from the severe lattice distortion of HEA, the sintering capacity of the binder is enhanced, consequently the liquid binder has the better dispersibility during sintering [33–35]. The uniform dispersion of binder phase can motivate to form many complete and moderate rim phases in cermets CH1 and CH2 (Fig. 3b and c), and wet the ceramic particles and enhance the bonding of ceramic phase [36]. But the uniformity of binder phase in cermet CH3 adding pure CrMnFeCoNi binder is reduced, thus bringing about the limited wetting of the hard phase.

3.2. *Mechanical properties*

Fig. 8 describes the mechanical properties of the four cermets. With increased HEA binder, the relative density of cermets gradually reduces from 99.17% to 98.37%. The Vickers hardness roughly increases with an increment of HEA binder. Additionally, the strength (TRS) and fracture toughness maintain the same change tendency of rising the peak and then falling. The cermet CH1 obtains a prominent mechanical property combination with hardness of 1646 ± 13.5 HV_{30}, strength (TRS) of 2181 ± 167.2 MPa and fracture toughness of 9.1 ± 0.11 MPa $m^{1/2}$ compared with the conventional cermet CH0.

The gas stored in the satellite structure and pores in dendritic structure of gas atomized HEA powders is incompletely released during sintering, which hinders the densification of samples [25]. Furthermore, the evaporation of low-melting point Mn element at the sintering temperature affects the densification process of cermets. In addition, the low wettability of pure CrMnFeCoNi HEA binders to ceramic phase leads to the poor densification of cermet CH3 [20]. Therefore, the relative density of sintered samples decreases gradually with the increment of HEA binder.

Table 3 – EDS analysis (at.%) performed on binder phases of four sintered cermets.

zone	cermet	Cr	Mn	Fe	Co	Ni	Ti	Mo + W + Ta
gray binder	CH0	–	–	–	–	64.61	28.92	6.47
	CH1	3.62	3.98	5.63	6.86	57.76	17.33	4.82
	CH2	6.17	7.74	12.29	13.50	44.21	13.41	2.68
	CH3	6.20	7.59	18.35	20.34	18.77	24.18	4.57

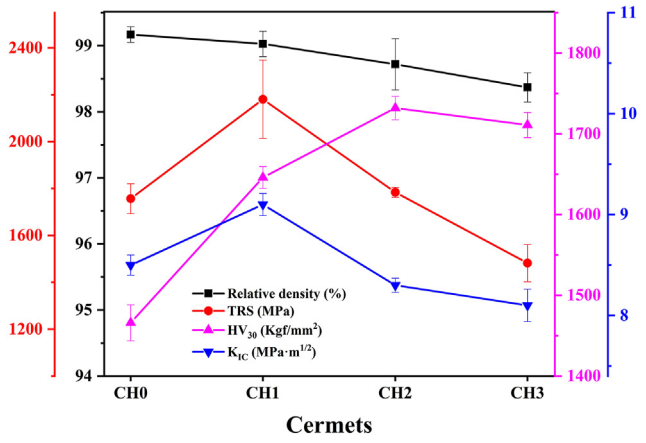

Fig. 8 – Mechanical properties of cermets CH0, CH1, CH2 and CH3.

In general, the hardness of Ti(C,N)–Co cermets is estimated as 1500–1700 HV, while the hardness of cermets adding HEA in this study is about 1650–1750 HV. The addition of CrMnFeCoNi binder with high inherent hardness inhibits the grain growth, and the appearance of finer grains means more grain boundary strengthening [37]. Meanwhile, the average free path of binder phase in cermets obtaining HEA (Fig. 7) falls compared with cermet CH0, usually resulting in an increment of hardness [31,32]. In addition, the hardness values of cermets are improved due to an enhanced solid solution strengthening.

Compared with the cermet CH0, the TRS value of cermet CH1 is greatly increased from 1757 ± 64.1 MPa to 2181 ± 167.2 MPa. The presence of complete and well-fined rim phases ensures the superior wettability of the binder phase on hard phase (Fig. 3b). In addition, the binder is uniformly dispersed in the cermets (Fig. 7b). Hence, the bonding strength between different phases is enhanced. However, as HEA is excessively added, the wettability of binder to hard particles is weakened. Simultaneously, the matrix density also reduces, the strength of cermets possesses a downward trend.

The cermet CH1 obtains higher fracture toughness of 9.1 ± 0.11 MPa $m^{1/2}$ compared with cermet CH0 of 8.5 ± 0.10 MPa $m^{1/2}$. The excellent fracture toughness of cermet CH1 can be ascribed to high deformability of the binder and its good wettability to hard phase. The HEA exhibits an excellent fracture strain, which can absorb the strain energy generated by external force, thereby the matrix can bear more impact energy before fracture, so toughening the cermet [14,31]. Moreover, the binder phase of cermet CH1 gains a uniform dispersion to maintain the high bonding strength towards ceramic phase.

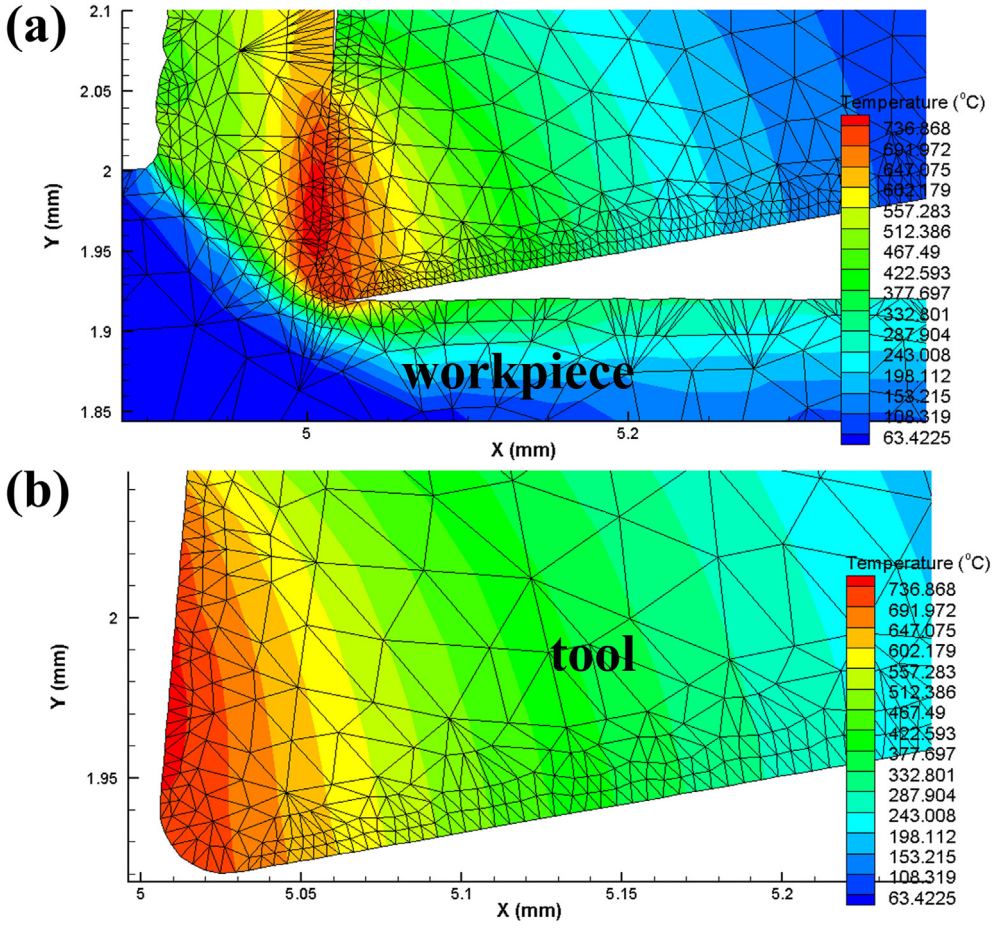

Fig. 9 – The cutting temperature distribution of inserts through Third Wave AdvantEdge.

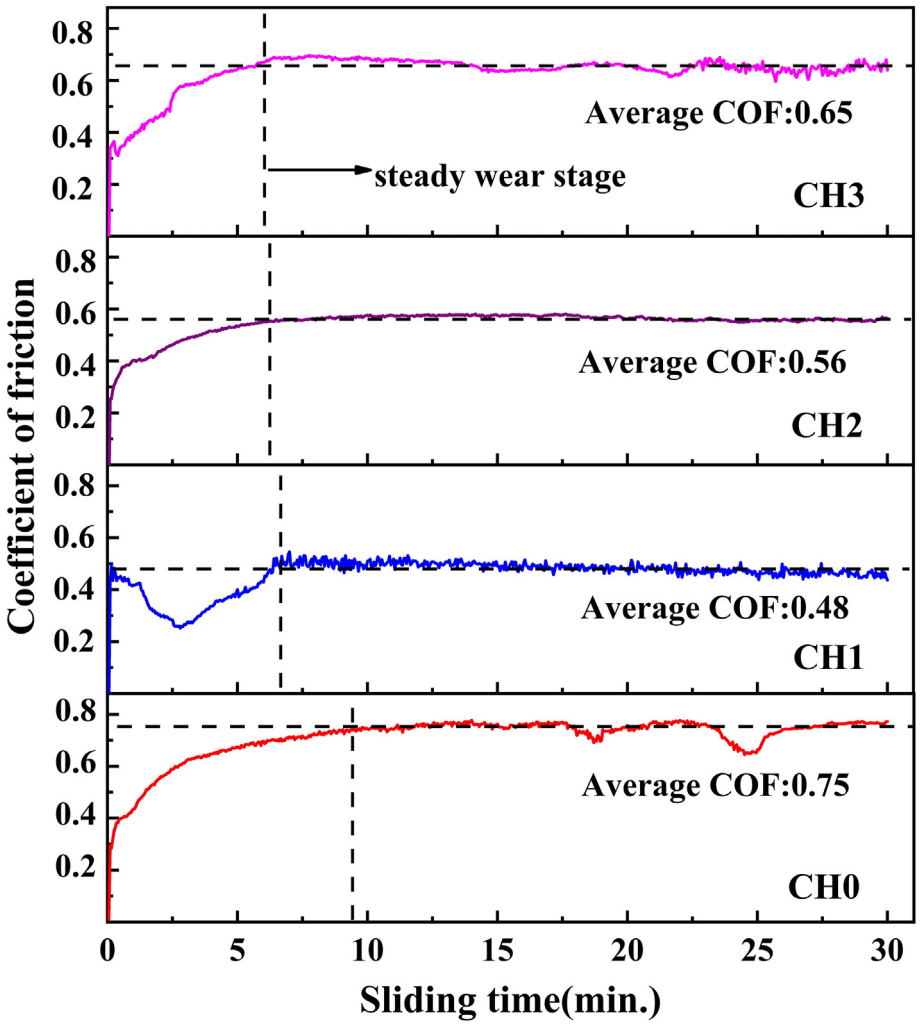

Fig. 10 – Friction coefficient (COF) curves of cermets at 750 °C.

3.3. *Tribological properties at high temperature*

As cutting tool materials, the tribological behavior of cermets under elevated temperature is inevitable, so the excellent wear resistance plays a crucial role to broaden their application fields [1]. The temperature field distribution of inserts during cutting 17-4 PH stainless steel is detected by Three Wave AdvantEdge. In Fig. 9b, the tool–chip interface temperature even exceeds 730 °C. Therefore, it is necessary to research the co-effects of CrMnFeCoNi/Ni binders on tribological performance of cermets under 750 °C. Friction coefficient (COF) curves of cermets at 750 °C are demonstrated in Fig. 10. It illustrates that the friction coefficient of all cermets rises rapidly at the beginning of tests, then reaches the steady wear stage after a certain time. Compared with cermet CH0, all average COF values of cermets CH1, CH2 and CH3 at 750 °C are relatively lower. With increased HEA binder content, the running-in time gradually decreases. The above results are indications that the addition of HEA binder can reduce COF values of cermets. It can be attributed to the excellent wear properties and thermal softening resistance of CrMnFeCoNi binder [38,39]. The improved hardness of cermets obtaining HEA binders to enhance lubrication and anti-abrasion properties is proposed to be an important reason for prominent wear resistance. The cermet CH1 possesses the lowest average friction coefficient at 750 °C about 0.48, indicating the best wear resistance properties.

Fig. 11 displays the results of wear surface profilometry and the depth profile at 750 °C. It clearly shows that cermet CH1 obtains the minimum wear depth and cross-sectional area of the worn scar, but the cermet CH0 possesses the maximum wear depth and cross-sectional area of worn scar. Fig. 12 illustrates the wear rates of sintered cermets after sliding tests at 750 °C. The wear rates of samples decrease first and then increase with the addition of HEA binder, which is similar to the change tendency of average COF (Fig. 10). The tribological characteristics of some Ti(C,N)-HEA cermets after sliding in dry conditions are listed in Table 4. Under these conditions, the COF values of cermets are lower compared against Si_3N_4 balls and the wear rates are 10^{-5}-10^{-6} $mm^3/N{\cdot}m$. At the present study, cermet CH1 possesses the lowest wear rate of 8.82×10^{-6} $mm^3/N{\cdot}m$ at high temperature. The wear rate of

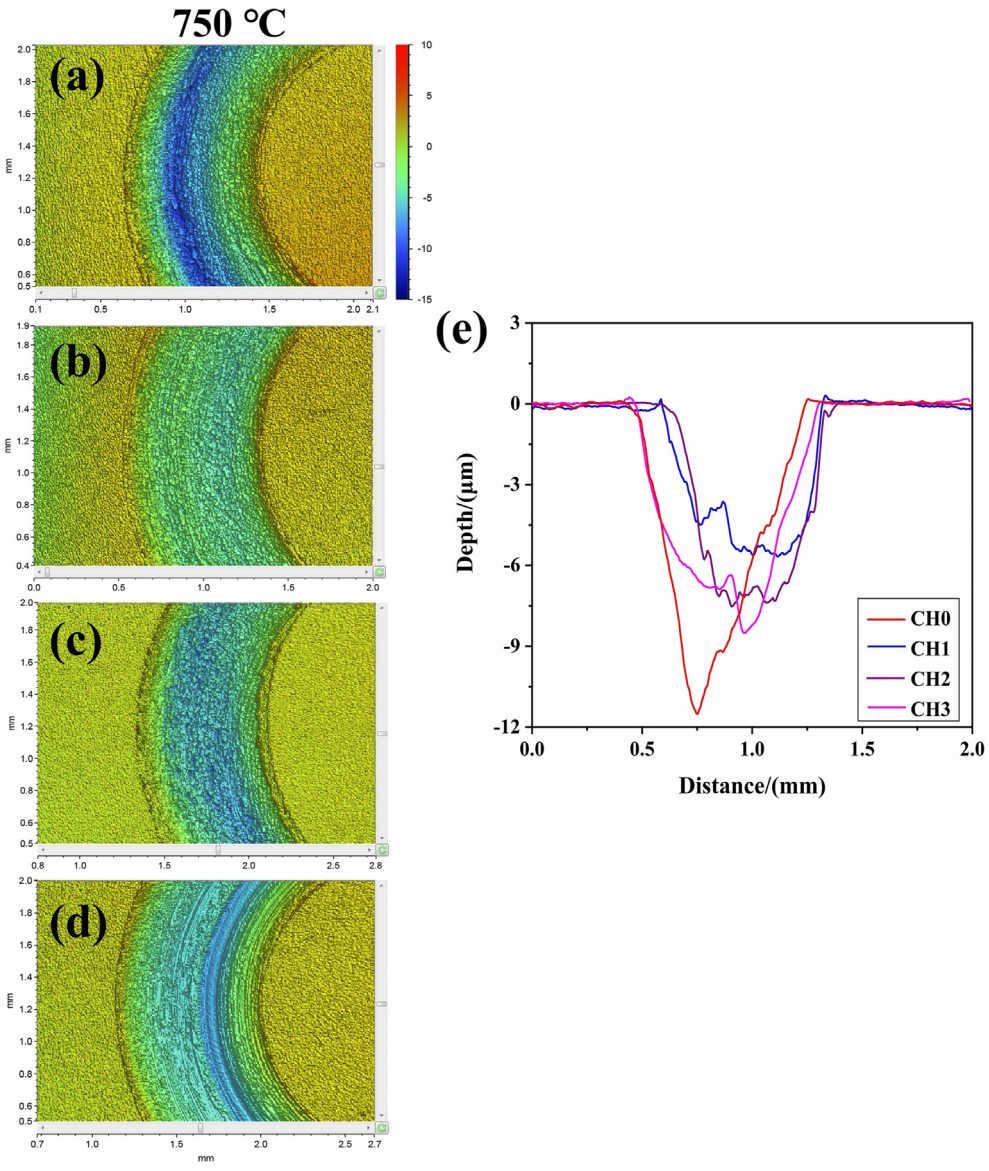

Fig. 11 – The wear surface profilometry of cermets after wear tests at 750 °C: (a) CH0; (b) CH1; (c) CH2; (d) CH3. (e) The depth profile of wear tracks after wear tests.

cermet CH0 is 1.52 × 10^{-5} $mm^3/N \cdot m$, which are 1.72 times, 1.30 times and 1.02 times of the wear rates of cermet CH1, CH2 and CH3, respectively.

The result implies that CrMnFeCoNi can reduce the wear rate of cermets at high temperature and accordingly enhance the wear resistance, meanwhile, the FCC binder combination of 10wt.% Ni-5wt.% HEA can significantly improve the wear resistance. The resistance of materials to friction and wear is closely related to their hardness and fracture toughness [9,40]. CrMnFeCoNi greatly improves the hardness of cermets (Fig. 8), which can resist plastic deformation and delamination. Generally speaking, the hardness of materials is in relation to

Table 4 – The lists of tribological characteristics of Ti(C,N)-based cermets during sliding in dry conditions.

Composition	Counterbody	Test conditions	COF	Wear rate ($mm^3/N \cdot m$)	References
Ti(C,N)-WC-Mo_2C–TaC–CoCrFeNiCu	Steel	1000 rpm, 10N, 600 °C/800 °C	0.21–0.38	10^{-6}–10^{-7}	[28]
Ti(C,N)-WC-Mo_2C–TaC–$Al_{0.3}$CoCrFeNi	Cemented carbide	200 rpm, 4.9N, 900 °C	0.13	–	[22]
Ti(C,N)-WC-Mo_2C-xNbC-CoCrFeNi	Steel	1000 rpm, 10N, 700 °C	0.2–0.29	10^{-5}–10^{-6}	[45]
Ti(C,N)–TiB_2–FeCoCrNiAl	Cemented carbide	450 rpm, 5N, 200–800 °C	0.23–0.36	-10^{-5}	[46]
Ti(C,N)-WC-Mo_2C–TaC-(Ni/CrMnFeCoNi)	Si_3N_4	1000 rpm, 10N, 750 °C	0.48–0.75	10^{-5}–10^{-6}	This study

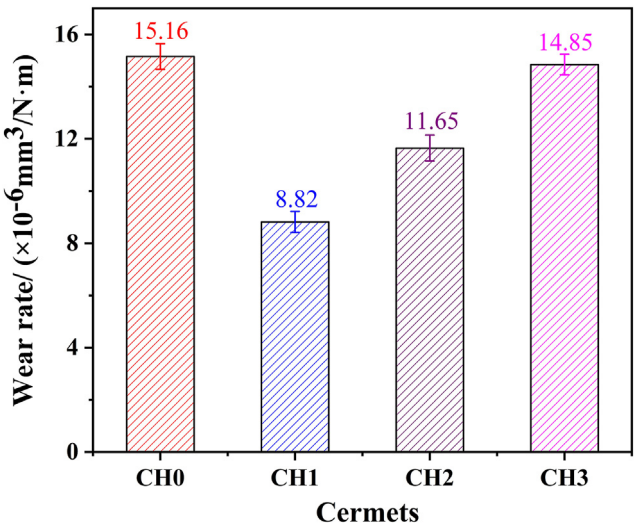

Fig. 12 – The wear rates of all cermets after wear tests at 750 °C.

the dislocation slip system [41,42]. The sliding wear is a thermo-mechanical action. During high-temperature sliding process, the dislocations are firstly formed in the soft binder whose evolution is mainly concentrated on grain boundaries (Fig. 7). For multi-principal component CrMnFeCoNi, the stacking fault energy is comparatively low, which facilities the generation of twins [22,43]. The formation of twins, lattice distortions from multi-component HEA binder and their related pinning effect hinder the motion of dislocations, enhancing the high-temperature hardness of matrixes. In addition, the solution hardening and low vacancy mobility from multi-principal element effect also conduces to improve high-temperature softening resistance [44]. However, the cermet CH3 containing excess low-wettability binder obtains low density and reduced fracture toughness, easily induces cracking, resulting in the pullout of ceramic grains, thus impeding high-temperature wear resistance. In fact, the best wear resistance of cermet CH1 also is ascribed to dense microstructure, a large number of complete and fine grains and improved fracture toughness.

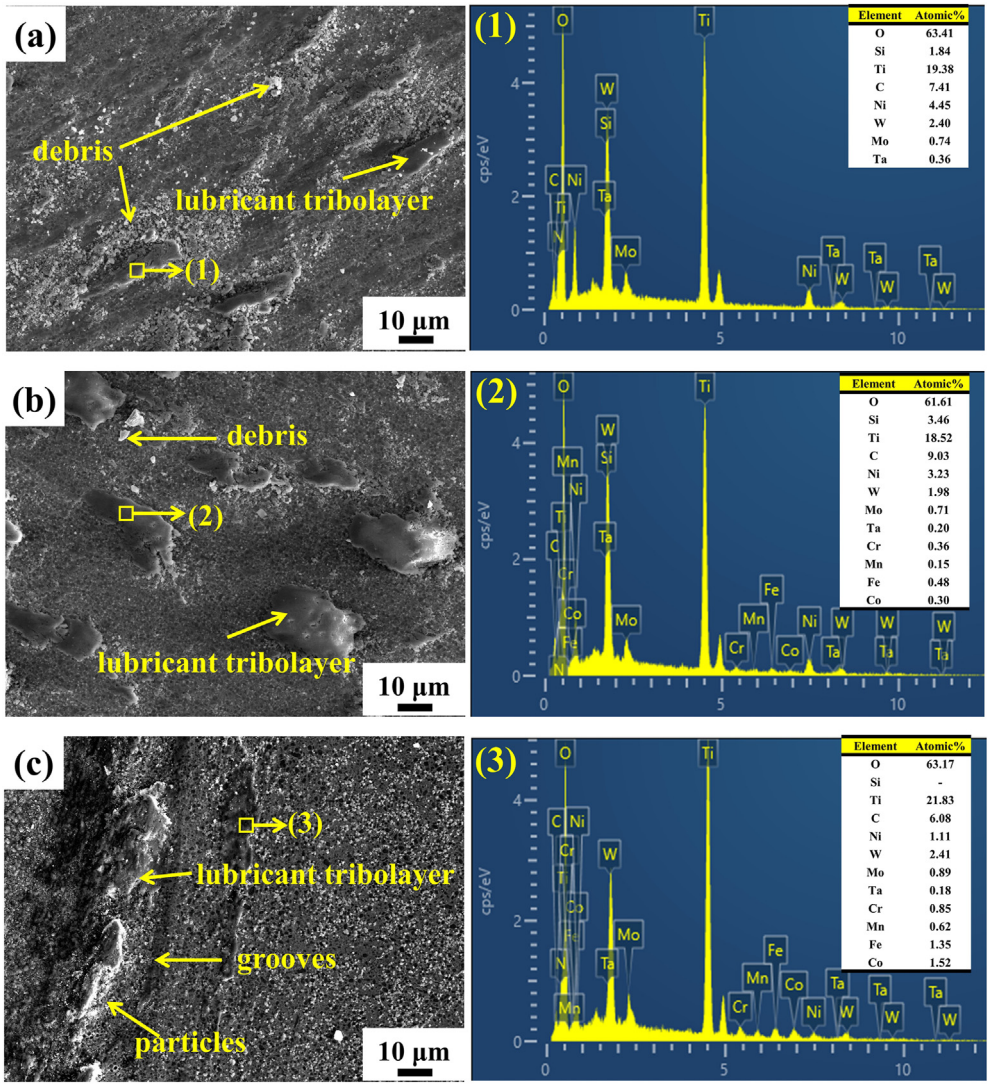

Fig. 13 – SEM images and EDS results of wear scars for cermets after sliding wear tests at 750 °C: (a) cermet CH0; (b) cermet CH1; (c) cermet CH3.

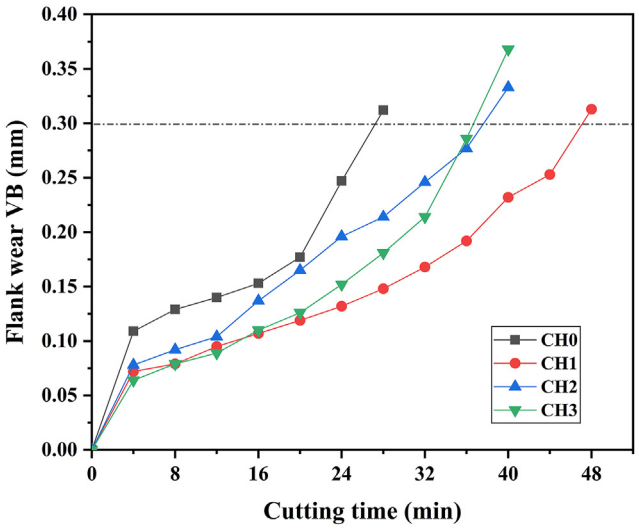

Fig. 14 – The flank wear values of cermet inserts with different binder contents.

To investigate the wear mechanisms of Ti(C,N)–Ni–CrMnFeCoNi cermets at high temperature, the wear morphologies and the corresponding EDS analyses are shown in Fig. 13. Wear debris and tribo-oxide layer appear in the morphology of cermet CH0 (Fig. 13a). The EDS result shows that the tribolayer is rich in O, Ti elements and a small amount of Ni, W and other elements (Figs. 1–13). At high temperature, the ceramic matrixes are significantly oxidized and the tribo-oxide layers are continuously removed after formation in the wear process. The abrasion of hard particles containing various oxides and the wear of debris lead to the high wear loss. It concludes that the wear mechanisms of cermet CH0 at high temperature are abrasive wear and the removal of tribochemical layers. For cermet CH1, the dense tribochemical layers are generated on the wear morphology, and only a small number of debris can be observed. Due to the excellent high-temperature hardness, refined grains and uniformly distributed and anti-softening binder phase, the ability of cermet CH1 to resist deformation at high temperature is strengthened. As a lubricant layer, dense and stable tribochemical layer can inhibit the wear of the matrix. The main wear mechanism of cermet CH1 is the removal of tribochemical layers. For cermet CH3, the particles, grooves and tribochemical layers are formed in Fig. 13c. The EDS result reveals that more hard phase elements Ti, Ta, Mo and W participate in the formation of tribochemical layers compared with cermets CH0 and CH1. Due to the insufficient wettability and low toughness, the deformed binder of cermet CH3 is easily smeared away during high-temperature sliding, and more ceramic particles are pulled out. Consequently, the lubricant layers are easy to be removed under the mechanical plowing action of abrasive particles and frictional stress [45]. Hence, the wear resistance of cermet CH3 at high temperature is almost no enhancement compared with cermet CH0. The wear mechanisms of cermet CH3 are mainly abrasive wear and the removal of tribochemical layers.

3.4. *Cutting properties of cermet inserts*

To investigate the cutting properties of the cermets, the inserts with different binders are used to cut 17-4 PH stainless steel under the dry machining conditions. Fig. 14 displays the change curve of the flank wear of various inserts. In the initial wear stage (the first 4 min), the inserts containing HEA show the lower flank wear values compared with insert CH0. Then, the flank wear value of insert CH0 increases sharply after 20 min and firstly reaches 0.3 mm. The insert CH1 basically maintains the minimum flank wear value under the same cutting time, and reaches the flank wear value of 0.3 mm after the longest machining time, which testifies to the outstanding cutting performance. The cutting lifetime of insert CH1 is increased by 70% compared with insert CH0.

Fig. 15 presents the flank wear morphologies of the three inserts after dry machining for 12 min. The build-up-edge (BUE), grooves, adhesion and chips appear in Fig. 15. The appearance of BUE would shorten the service life of tools and reduce surface quality of workpieces [47]. During high-speed dry machining, the particles would be pulled out from the tool matrix due to the severe plastic deformation, and would exist between the tool and the processed material as abrasive particles. The abrasive particles scratch the tool surface during cutting, generating grooves in the flank area of all inserts. It indicates that there is the abrasive wear at a different degree in cutters. The insert CH0 (Fig. 15a) exhibits a large wear width and severe BUE in comparison the other inserts. The insert CH1 (Fig. 15b) acquires the better cutting performance than insert CH0 , exhibiting a narrow and stable flank wear boundary, and relatively few grooves. It is contributed to the excellent high-temperature wear properties and thermal softening resistance owing to adding 5wt.% CrMnFeCoNi binders in cermets. However, the chips occur in insert CH3 (Fig. 15c) due to insufficient strength and toughness of cermets adding excessive HEA binders.

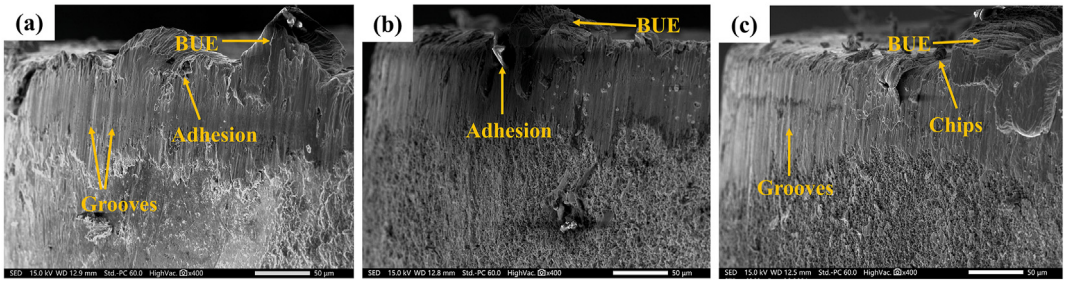

Fig. 15 – The Flank wear morphologies of inserts: (a) CH0; (b) CH1; (c) CH3.

4. Conclusions

Four kinds of Ti(C,N)-based cermets were fabricated by regulating the content of CrMnFeCoNi and Ni binders. The co-effects of CrMnFeCoNi/Ni binders on the microstructure, mechanical, wear resistance and cutting properties of cermets were investigated. The main conclusions are as follows:

(1) Because of the sluggish diffusion effect of CrMnFeCoNi binder, the grain growth of cermets containing HEA binder is markedly inhibited compared with Ti(C,N)–Ni cermets. The single FCC binder phases of cermets with CrMnFeCoNi/Ni binders are uniformly dispersed, motivating to form many complete and moderate rim phases and wet the ceramic particles.
(2) The hardness of cermets roughly increases with an increment of CrMnFeCoNi, while the strength (TRS) and fracture toughness maintain the change tendency of rising the peak and then falling with CrMnFeCoNi additions. Ti(C,N)-5wt.% CrMnFeCoNi-10wt.% Ni cermets obtains a prominent mechanical property combination with hardness of 1646 ± 13.5 HV_{30}, strength (TRS) of 2181 ± 167.2 MPa and fracture toughness of 9.1 ± 0.11 MPa $m^{1/2}$ by using a co-effect between the good wettability of uniformly dispersed FCC binder and the sluggish diffusion effect of HEA additions. However, Ti(C,N)–CrMnFeCoNi cermets gain a low strength (TRS) and insufficient fracture toughness in comparison Ti(C,N)–Ni cermets due to the high residual porosity.
(3) The cermets containing CrMnFeCoNi/Ni binders obtain reduced friction coefficients and decreased wear rates at high temperature compared with Ti(C,N)–Ni cermets and Ti(C,N)-HEA cermets. The superior high-temperature wear resistance can be ascribed to the thermal softening resistance of CrMnFeCoNi, strengthening and toughening effect of CrMnFeCoNi/Ni binders on matrix and the transition of the wear mechanisms from abrasive wear and the removal of tribochemical layers to the removal of tribochemical layers. However, the cermet CH3 containing excess HEA binder obtains low density and reduced fracture toughness, easily induces cracking, resulting in the pullout of ceramic grains, thus weakening the wear resistance at high temperature. Furthermore, the cutting lifetime of cermets adding 5wt.% HEA-10wt.% Ni binders is increased by 70% in comparison with Ti(C,N)–Ni cermets during machining 17-4 PH stainless steel. Concisely, Ti(C,N)-based cermets with outstanding wear resistance and cutting performance can be obtained by partially replacing Ni binder with 5–10 wt.% CrMnFeCoNi.

Declaration of Competing Interest

The authors declare that they have no known competing financial interests or personal relationships that could have appeared to influence the work reported in this paper.

Acknowledgements

This research is financially supported by the Science and Technology Major Project of Sichuan Province (No. 2020ZDZX0022), SCU-Zi Gong Project (No.2019CDZG-1) and Sichuan Province Science and Technology Support Program (2021JDTD0025). We appreciate Wang Hui and Shuping Zheng from the Analytical & Testing Center of Sichuan University for their help with SEM and EBSD characterization. The authors honestly thank the Chengdu Mingwu Technology Corp., Ltd. of China.

REFERENCES

[1] Liu N, Chao S, Yang H. Cutting performances, mechanical property and microstructure of ultra-fine grade Ti(C,N)-based cermets. Int J Refract Metals Hard Mater 2006;24:445–52.
[2] Zheng Y, You M, Xiong W, Liu W, Wang S. Valence-electron structure and properties of main phases in Ti(C, N)-based cermets. Mater Chem Phys 2003;82:877–81.
[3] Wan W, Xiong J, Li Y, Tang Q, Liang M. Erosion-corrosion behavior of Ti(C,N)-based cermets containing different secondary carbides. Int J Refract Metals Hard Mater 2017;66:180–7.
[4] Liu J, Ji X, Guo Z, Qin C, Xiao Y, You Q. Characteristics and cutting performance of the CVD coatings on the TiCN-based cermets in turning hardened AISI H13 steel. J Mater Res Technol 2020;9:1389–99.
[5] Zhao XZ, Liu JJ, Zhu BL, Miao HZ, Luo ZB. Friction and wear of Si3N4 ceramic/stainless steel sliding contacts in dry and lubricated conditions. J Mater Eng Perform 1997;6:203–8.
[6] Monteverde F, Bellosi A. Oxidation behavior of titanium carbonitride based materials. Corrosion Sci 2002;44:1967–82.
[7] Dios M, Kraleva I, González Z, Alvaredo P, Ferrari B, Gordo E, et al. Mechanical characterization of Ti(C,N)-based cermets fabricated through different colloidal processing routes. J Alloys Compd 2018;732:806–17.
[8] Xu Q, Ai X, Zhao J, Gong F, Pang J, Wang Y. Effects of metal binder on the microstructure and mechanical properties of Ti(C,N)-based cermets. J Alloys Compd 2015;644:663–72.
[9] Rajabi A, Ghazali MJ, Syarif J, Daud AR. Development and application of tool wear: a review of the characterization of TiC-based cermets with different binders. Chem Eng J 2014;255:445–52.
[10] Liu N, Xu Y, Li Z, Chen M, Li G, Zhang L. Influence of molybdenum addition on the microstructure and mechanical properties of TiC-based cermets with nano-TiN modification. Ceram Int 2003;29:919–25.
[11] Yeh JW, Chen SK, Lin SJ, Gan JY, Chin TS, Shun TT, et al. Nanostructured high-entropy alloys with multiple principal elements: novel alloy design concepts and outcomes. Adv Eng Mater 2004;6:299–303.
[12] Zhu G, Liu Y, Ye J. Fabrication and properties of Ti(C,N)-based cermets with multi-component AlCoCrFeNi high-entropy alloys binder. Mater Lett 2013;113:80–2.
[13] Mueller-Grunz A, Alveen P, Rassbach S, Useldinger R, Moseley S. The manufacture and characterization of WC-(Al)CoCrCuFeNi cemented carbides with nominally high entropy alloy binders. Int J Refract Metals Hard Mater 2019;84:105032.
[14] Luo W, Liu Y, Shen J. Effects of binders on the microstructures and mechanical properties of ultrafine WC-10%AlxCoCrCuFeNi composites by spark plasma sintering. J Alloys Compd 2019;791:540–9.

[15] Zhou PL, Xiao DH, Zhou PF, Yuan TC. Microstructure and properties of ultrafine grained AlCrFeCoNi/WC cemented carbides. Ceram Int 2018;44:17160–6.
[16] Velo IL, Gotor FJ, Alcalá MD, Real C, Córdoba JM. Fabrication and characterization of WC-HEA cemented carbide based on the CoCrFeNiMn high entropy alloy. J Alloys Compd 2018;746:1–8.
[17] Holmström E, Lizárraga R, Linder D, Salmasi A, Wang W, Kaplan B, et al. High entropy alloys: substituting for cobalt in cutting edge technology. Appl Mater Today 2018;12:322–9.
[18] Zhang Y, Zuo TT, Tang Z, Gao MC, Dahmen KA, Liaw PK, et al. Microstructures and properties of high-entropy alloys. Prog Mater Sci 2014;61:1–93.
[19] Zhu G, Liu Y, Ye J. Early high-temperature oxidation behavior of Ti(C,N)-based cermets with multi-component AlCoCrFeNi high-entropy alloy binder. Int J Refract Metals Hard Mater 2014;44:35–41.
[20] de la Obra AG, Avilés MA, Torres Y, Chicardi E, Gotor FJ. A new family of cermets: chemically complex but microstructurally simple. Int J Refract Metals Hard Mater 2017;63:17–25.
[21] de la Obra AG, Sayagués MJ, Chicardi E, Gotor FJ. Development of Ti(C,N)-based cermets with (Co,Fe,Ni)-based high entropy alloys as binder phase. J Alloys Compd 2020;814:152218.
[22] Fang Y, Chen N, Du G, Zhang M, Zhao X, Cheng H, et al. High-temperature oxidation resistance, mechanical and wear resistance properties of Ti(C,N)-based cermets with Al0.3CoCrFeNi high-entropy alloy as a metal binder. J Alloys Compd 2020;815:152486.
[23] Dong D, Xiang X, Huang B, Xiong H, Zhang L, Shi K, et al. Microstructure and properties of WC-Co/CrMnFeCoNi composite cemented carbides. Vacuum 2020;179:109571.
[24] Schubert WD, Neumeister H, Kinger G, Lux B. Hardness to toughness relationship of fine-grained WC-Co hardmetals. Int J Refract Metals Hard Mater 1998;16:133–42.
[25] Wang P, Huang P, Ng FL, Sin WJ, Lu S, Nai MLS, et al. Additively manufactured CoCrFeNiMn high-entropy alloy via pre-alloyed powder. Mater Des 2019;168:107576.
[26] Laurent-Brocq M, Perrière L, Pirès R, Champion Y. From high entropy alloys to diluted multi-component alloys: range of existence of a solid-solution. Mater Des 2016;103:84–9.
[27] Peng Y, Miao H, Peng Z. Development of TiCN-based cermets: mechanical properties and wear mechanism. Int J Refract Metals Hard Mater 2013;39:78–89.
[28] Wang Z, Xiong J, Guo Z, Yang T, Liu J, Chai B. The microstructure and properties of novel Ti(C,N)-based cermets with multi-component CoCrFeNiCu high-entropy alloy binders. Mater Sci Eng, A 2019;766:138345.
[29] Singh AK, Subramaniam A. On the formation of disordered solid solutions in multi-component alloys. J Alloys Compd 2014;587:113–9.
[30] Yang Q, Xiong W, Zhang G, Huang B. Grain growth in Ti(C,N)-Based cermets during liquid-phase sintering. J Am Ceram Soc 2015;98:1005–12.
[31] Yadav S, Zhang Q, Behera A, Haridas RS, Agarwal P, Gong J, et al. Role of binder phase on the microstructure and mechanical properties of a mechanically alloyed and spark plasma sintered WC-FCC HEA composites. J Alloys Compd 2021:160265.
[32] Emani SV, Wang C, Shaw LL, Chen Z. On the hardness of submicrometer-sized WC–Co materials. Mater Sci Eng, A 2015;628:98–103.
[33] Vaidya M, Trubel S, Murty BS, Wilde G, Divinski SV. Ni tracer diffusion in CoCrFeNi and CoCrFeMnNi high entropy alloys. J Alloys Compd 2016;688:994–1001.
[34] Yang T, Cai B, Shi Y, Wang M, Zhang G. Preparation of nanostructured CoCrFeMnNi high entropy alloy by hot pressing sintering gas atomized powders. Micron 2021;147:103082.
[35] Zhang M, Zhang W, Liu F, Peng Y, Hu S, Liu Y. Effect of binding and dispersion behavior of high-entropy alloy (HEA) powders on the microstructure and mechanical properties in a novel HEA/diamond composite. Entropy 2018;20:924.
[36] Dong D, Yang W, Xiong H, Zhang L, Shi K, Liao J. Ti(C,N)-based cermets with fine grains and uniformly dispersed binders: effect of the Ni–Co based binders. Ceram Int 2020;46:6300–10.
[37] Xiao LL, Zheng ZQ, Guo SW, Huang P, Wang F. Ultra-strong nanostructured CrMnFeCoNi high entropy alloys. Mater Des 2020;194:108895.
[38] Joseph J, Haghdadi N, Shamlaye K, Hodgson P, Barnett M, Fabijanic D. The sliding wear behaviour of CoCrFeMnNi and AlxCoCrFeNi high entropy alloys at elevated temperatures. Wear 2019;428–429:32–44.
[39] Joseph J, Haghdadi N, Annasamy M, Kada S, Hodgson PD, Barnett MR, et al. On the enhanced wear resistance of CoCrFeMnNi high entropy alloy at intermediate temperature. Scripta Mater 2020;186:230–5.
[40] Kumar BVM, Basu B, Vizintin J, Kalin M. Tribochemistry in sliding wear of TiCN–Ni-based cermets. J Mater Res 2008;23:1214–27.
[41] Bolognini S, Feusier G, Mari D, Viatte T, Benoit W. TiMoCN-based cermets: high-temperature deformation. Int J Refract Metals Hard Mater 2003;21:19–29.
[42] Milman YV, Chugunova SI, Goncharova IV, Chudoba T, Lojkowski W, Gooch W. Temperature dependence of hardness in silicon–carbide ceramics with different porosity. Int J Refract Metals Hard Mater 1999;17:361–8.
[43] Rogal A, Kalita D, Tarasek A, Bobrowski P, Czerwinski F. Effect of SiC nano-particles on microstructure and mechanical properties of the CoCrFeMnNi high entropy alloy. J Alloys Compd 2017;708:344–52.
[44] Hsu C, Juan C, Wang W, Sheu T, Yeh J, Chen S. On the superior hot hardness and softening resistance of AlCoCrxFeMo0.5Ni high-entropy alloys. Mater Sci Eng, A 2011;528:3581–8.
[45] Gou Q, Xiong J, Guo Z, Liu J, Yang L, Li X. Influence of NbC additions on microstructure and wear resistance of Ti(C,N)-based cermets bonded by CoCrFeNi high-entropy alloy. Int J Refract Metals Hard Mater 2021;94:105375.
[46] Li Z, Fu P, Hong C, Chang F, Dai P. Tribological behavior of Ti(C, N)-TiB2 composite cermets using FeCoCrNiAl high entropy alloys as binder over a wide range of temperatures. Mater Today Commun 2021;26:102095.
[47] Lim GH. Tool-wear monitoring in machine turning. J Mater Process Technol 1995;51:25–36.